

A Global View of the Wind Sea and Swell Waves Interannual Variability from ERA-40

Alvaro Semedo^{1,2}

Kay Sušelj³

¹ Department of Earth Sciences – Meteorology
Uppsala University
Uppsala – Sweden
E-mail: alvaro.semedo@met.uu.se

² Risø - DTU National Laboratory for Sustainable Energy
Technical University of Denmark
Roskilde - Denmark

³ ForWind, Center for Wind Energy Research
Carl von Ossietzky University
Oldenburg - Germany

1. Introduction

Ocean surface waves are one of the most obvious and fundamental phenomena present at the air-sea interface. In terms of energy the ocean wave spectrum is dominated by surface gravity waves (Munk, 1951). Therefore most of the theoretical and experimental studies available in the scientific literature are focused on surface gravity waves (henceforth simply called “waves”): their generation, evolution and propagation, and interaction with the oceanic and the atmospheric environment.

There are two types of waves in the ocean surface. During the generation and growing processes, when waves are considered young, they are designated as wind sea. As they propagate away from their generation area, or when their phase speed is higher than the overlying wind speed, they are called swell. Since swell propagates from one place to the other, in the open ocean the wave field at a given time and place is, most of the times, the result of contributions from waves with different frequencies and directions, reflecting different origins and ages.

Recently there has been a renewed interest in the study of swell, ranging from swell propagation and attenuation (Ardhuin *et al.*, 2009), to the swell impact on the marine atmospheric boundary layer – MABL –, (Smedman *et al.*, 1999; Sullivan *et al.*, 2008; Smedman *et al.*, 2009; Högström *et al.*, 2009). It has been shown that swell decay rates can be affected by a reverse momentum flux process (Donelan *et al.*, 1997; Grachev and Fairall, 2001), occurring as swell performs work on the overlying atmosphere as it propagates faster than the wind (Semedo *et al.*, 2009). Swell can also be damped as it propagates trough

turbulent areas, by transferring energy into turbulent kinetic energy and enhancing the mixing processes in the upper ocean (Ardhuin and Jenkins, 2006; Kantha, 2006). The degree to which these processes cancel each other or add up is still unknown (Alves 2006; F. Ardhuin, personal communication). The fact that the physical mechanisms responsible for the swell attenuation still remain poorly understood, makes wave forecasting a difficult task in strongly swell dominated wave fields, like in the lower latitudes.

Recent wave climatology studies (e.g., Young, 1999; and Sterl and Caires, 2005) were focused on the most important wave parameters: the significant wave height, and wave period. However these two wave parameters give only a limited description of the wave field characteristics. Wave conditions in different areas may be similar in the sense that the significant wave height and period are equal, but they may still be very different in detail: a mixed sea state of wind sea and swell may have the same significant wave height and period as a slightly higher wind sea without swell. To distinguish such conditions, additional information about the significant wave height and period (and propagating directions) for wind sea and swell, separately, is needed (Holthuijsen, 2007).

Chen *et al.* (2002), using a combination between satellite altimetry and model hindcast wave data, and Gulev *et al.* (2003) and Gulev and Grigorieva (2006), using visual wave estimates from voluntary observing ships (VOS), complemented the existing wave climatologies by highlighting the differences between the two wave regimes. (These papers will henceforth be designated as CEFF02, GGSW03, and GG06, respectively.) Spectral partitioning is the best way to isolate wind sea and swell characteristics at a given location (Gerling, 1992; Hanson and Philips, 2001). Although wave spectra are available from *in situ* measurements (from buoys), and satellite synthetic aperture radars (SAR), these are not widely used in practice. On the other hand the separation between wind sea and swell heights is dependent on the human observer subjective judgment and experience. A global spectral description of the wave field, with a long enough time series, is only available from model results, like the European Centre for Medium-Range Weather Forecasts (ECMWF) ERA-40 wave reanalysis.

This study presents a detailed and qualitative study of the global wave field based on ERA-40, complementing previous studies (mainly CEFF02, GGSW03, and GG06). The global distribution of wind sea and swell significant wave heights (H_s^w and H_s^s), based on the wave spectra partition, are presented for the first time. The global spatial patterns of the leading modes of the overall significant wave height (H_s), and of H_s^w and H_s^s , respectively are studied using Empirical Orthogonal Functions (EOF) analysis. The first principal components are correlated with atmospheric indices to investigate the atmospheric forcing behind the variability of H_s , H_s^w and H_s^s .

2. Data and methods of analysis

2.1 ERA-40

The ERA-40 data set is a global reanalysis of meteorological observations from September 1957 to August 2002 (45 years), produced by the ECMWF (Uppala *et al.* 2005). The data set consist of 6-hourly fields (at synoptic times) with a $1.5^\circ \times 1.5^\circ$ grid resolution, covering the whole globe. Besides atmospheric variables, it also includes wave parameters. The ERA-40 is the first global reanalysis produced using a wave model coupled to a general circulation model. The wave model used in the coupled system is the state-of-the-art third generation WAM model (WAMDI Group, 1988). The ERA-40 wave data, due to changes in the assimilated data, is not completely homogeneous in time, and has four different periods clearly identified (Sterl and Caires, 2005). In one of these periods (from December 1991 to May 1993) erroneous remote sensing data was assimilated into the analyses process giving rise to corrupted wave model output. We choose not to use data from this period in our analysis.

In ERA-40 low wave heights tend to be overestimated, and high wave heights tend to be underestimated. This feature is a global characteristic of the ERA-40, and not a peculiarity of a particular location (Sterl and Caires, 2005). The validation of ERA-40 with buoy data indicate that the data describes the mean wave periods rather well, having a root-mean-square-error (rmse) most of the times bellow 1 s (Caires and Sterl, 2005). Sterl and Caires (2005) produced a statistically corrected wave height data set (the C-ERA40), using buoy data. The H_s was the only parameter corrected, and further used to produce a wave atlas. The H_s^w and H_s^s were not corrected, since that would not have been possible by using regular statistical tools. Correcting H_s^w and H_s^s would have implied correcting the modeled wave spectra itself, and that is an almost impossible task, since wave spectra buoy measurements are still scarce, and even more with collocated (or at least in the vicinity) wind speed observations. We are therefore left with the only choice of using “uncorrected” wind sea and swell parameters.

2.2 Wave parameters

The WAM model output is the two-dimensional wave energy spectrum $F(f, \theta)$ (f is frequency and θ is direction), obtained at each grid point by integrating the wave energy balance equation (Komen *et al.* 1994). From these spectra several derived integrated wave parameters can be obtained. The significant wave height (SWH) concept was originally defined by Munk (1945) as the “mean of the highest one-third of all individual waves in a record”. The mean variance of the sea-surface elevation (the *zeroth* moment) is statistically related to the significant wave height: $SWH \simeq H_s = 4.04 \sqrt{m_0}$, where $m_0 = \iint f^0 F(f, \theta) df d\theta$ is the variance or the zeroth moment. By weighting $F(f, \theta)$, the mean wave (propagation) direction is defined in the WAM model as $\theta_m = \text{atan}(SF / CF)$, where

$SF = \iint \sin(\theta)F(f,\theta)dfd\theta$ and $CF = \iint \cos(\theta)F(f,\theta)dfd\theta$. The significant wave heights, and mean wave directions of the wind sea waves (H_s^w, θ_m^w) and swell waves (H_s^s, θ_m^s) are computed by separating the one-dimensional (1D) spectrum into a wind sea and a swell components. The separation frequency is defined as the frequency corresponding to the wave phase speed \hat{c} where $33.6 \times (u_* / \hat{c}) \cos(\theta - \varphi) = 1$, and u_* is the friction velocity.

3. Climatology of the global wave field characteristics

The 6-hourly gridded values of the ERA-40 wave parameters were processed to yield monthly means, which latter were combined into seasonal means. Space limitations preclude the display of the results for the four seasons, therefore the focus will be on the extreme seasons DJF (December, January and February) and JJA (June, July and August).

Figure 1 displays the seasonal maps of the global climatological means of the U_{10} (wind speed at 10 m) fields, for DJF and JJA, respectively. The arrows represent the DJF and JJA means of φ (wind direction). The DJF and JJA U_{10} fields are characterized by high values in the extratropical areas and low values in the tropics, in both hemispheres. The distribution of U_{10} is not symmetric when the same seasons from both hemispheres are compared. Additionally the meridional decrease in wind speed from high to low latitudes is not monotonic. The U_{10} seasonal variability in the North Hemisphere (NH), particularly in the North Atlantic, is greater than in the South Hemisphere (SH). The Southern Ocean U_{10} maxima, in DJF and JJA, is located in its Indian sector, in the extratropical area. Equatorial regions are calm during all year, with almost no seasonal variability. Some mesoscale U_{10} features have a potential impact on the local to global wave field: the California, Peruvian, Namibian, and Somali low level coastal jets, which peak in the respective hemisphere summer, and the Indian Ocean monsoon. The intensification of the marine winds along the North flank of the South Indian Ocean High, during JJA, has a significant impact in the Indian Ocean wave field as well.

The seasonal maps of the global climatological means of the H_s , H_s^s , and H_s^w fields are shown in Figures 2 and 3. The arrows represent the DJF and JJA means of θ_m , θ_m^s , and θ_m^w . The highest H_s conditions are found along the extratropical areas in both hemispheres (Figures 2A and 3A). The H_s maxima in the SH are located in the Southern Ocean Indian sector, and range from 3.6 to 4.7 m, from DJF and JJA, respectively. In the Southern Ocean Pacific and Atlantic sectors, in the same seasons, the H_s maxima vary from 3.6 to 4.5 m and 3.4 to 3.9 m, respectively. In the North Atlantic and North Pacific the H_s maxima in JJA and DJF vary from 1.9 to 4.3 m and from 2.3 to 4.1. The North Pacific H_s

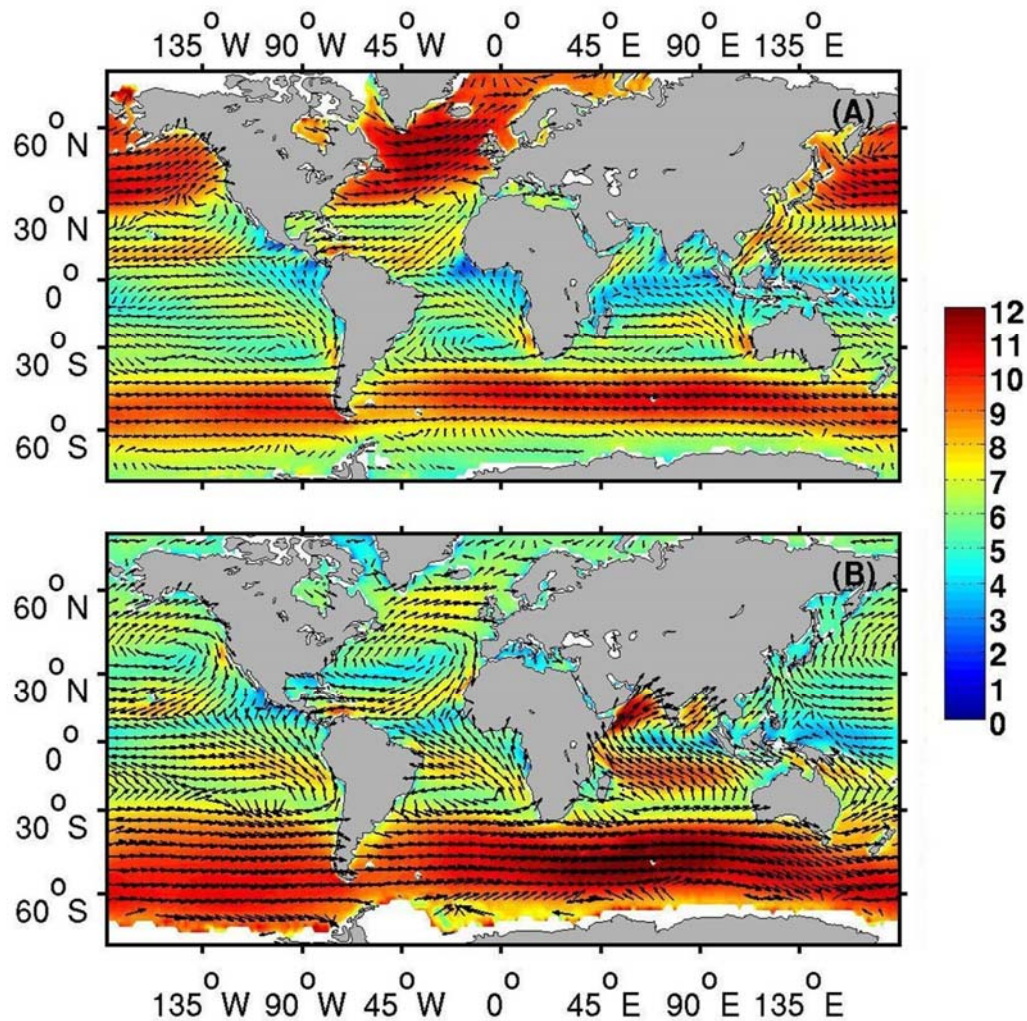


Figure 1 - Seasonal averages of U_{10} (ms^{-1}) and ϕ ($^{\circ}$) for DJF(A) and JJA (B). The arrows are scaled with background field.

maxima in JJA is located off the West coast of United States, due to the summer coastal wind speed enhancement, combined with swell waves generated in the Southern Ocean, and swell waves generated in the North Pacific.

The highest H_s^s (Figures 2B and 3B) are found during the respective hemisphere winter, along the extratropical areas. In the North Atlantic and North Pacific the H_s^s maxima vary, from JJA to DJF, from 1.7 to 3.3 m, and 2.0 to 3.2 m, respectively. In the Southern Ocean the highest H_s^s values are also found along the Indian sector, varying from DJF to JJA, from 2.8 to 3.7 m. In the Pacific

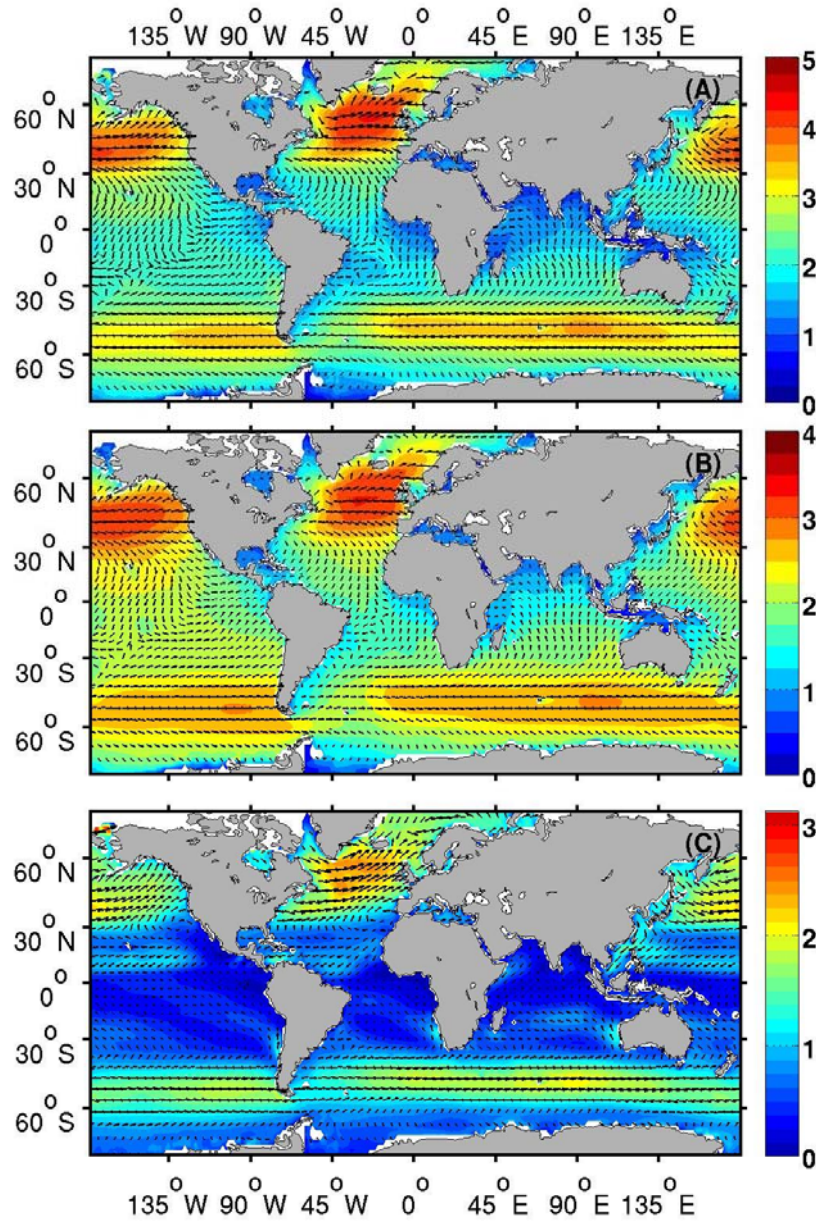


Figure 2 - Seasonal averages for DJF of H_s (m) and θ_m ($^\circ$) (A), H_s^S (m) and θ_m^S ($^\circ$) (B), and H_s^W (m) and θ_m^W ($^\circ$) (C). The arrows are scaled with background fields. The color scales vary between the sub-figures.

high U_{10} areas, in the extratropical areas, in the respective hemisphere winter. The lowest H_s^W are found in the tropics, with values close to zero, independently of the season. During DJF the H_s^W maxima in the North Atlantic and North Pacific extratropical areas are 2.5 and 2.2 m, respectively. Also in DJF, although summer in the SH, along the Southern Ocean Indian sector, the H_s^W maximum (2.1 m) is almost as high as in the North Pacific. In JJA, in the Southern Ocean

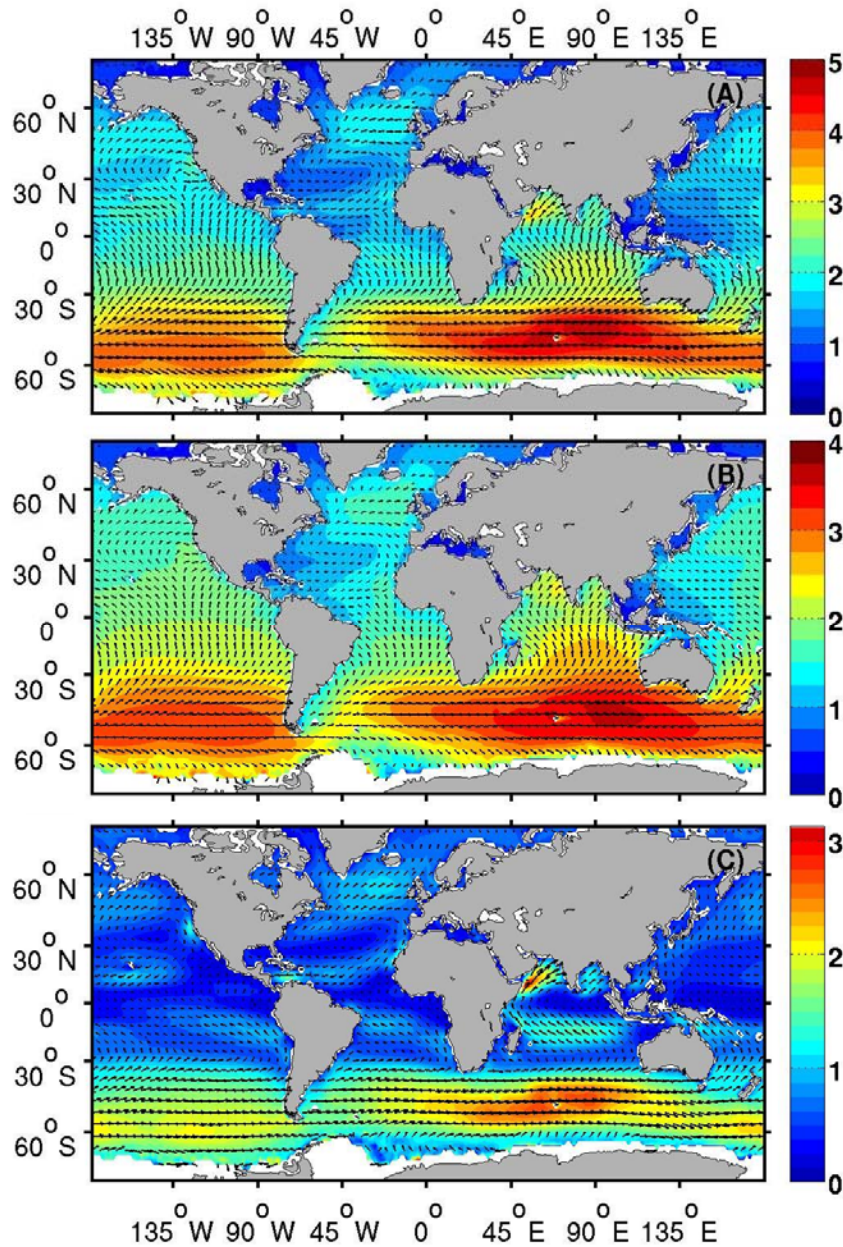


Figure 3 - Seasonal averages for JJA of H_s (m) and θ_m ($^\circ$) (A), H_s^s (m) and θ_m^s ($^\circ$) (B), and H_s^w (m) and θ_m^w ($^\circ$) (C). The arrows are scaled with background fields. The color scales vary between the sub-figures.

Indian sector, the H_s^w maximum is 2.8 m. In the Southern Ocean Pacific and Atlantic sectors the H_s^w maximum is, in DJF and JJA, 2.0 and 2.4 m, and 1.9 and 2.2 m, respectively. In JJA, in the NH summer, the H_s^w values along the extratropical storm tracks are 1.1 m in the North Atlantic, and 0.9 m in the North Pacific.

A general feature of the H_s^w and U_{10} fields is their collocation, reflecting the coupling between both fields. The spatial patterns of H_s and H_s^s in the extratropical areas in both hemispheres, are most of the times shifted eastward with respect to those of H_s^w , reflecting the swell propagation effect. In terms of wind and wave propagating direction, the alignment between φ and θ_m^w is very high almost every where, corresponding also to the high coupling

between the wind sea and the local wind fields during the wave growth process. This is not the case when φ and θ_m^s are compared, since swell waves are misaligned with the local wind direction. The relative angles between φ and θ_m^w and φ and θ_m^s fields in DJF and JJA were computed (not shown here). In the extratropical areas of both hemispheres, wind sea and swell waves are more or less aligned with the wind direction. Elsewhere, while the agreement between φ and θ_m^w still prevails, the relative angle between φ and θ_m^s can be very high, sometimes close to 180° , representing the decoupling between swell waves and the local wind field. In DJF and JJA the differences between φ and θ_m^s are greatest along the Pacific coast of Central America, where φ and θ_m^s are practically opposite, and the tropical and subtropical latitudes of all Oceans. In the Arabian Sea, in DJF, these differences are also very high. Since the H_s and θ_m fields are dominated by swell, the differences between φ and the total wave field mean wave direction (θ_m) are practically the same as between φ and θ_m^s .

4. EOF analysis

To obtain the structure of the main patterns of variability of the wave field, an EOF analysis (e.g. von Storch and Zwiers 1999) was carried out to the H_s , H_s^s and H_s^w detrended seasonal mean fields. To eliminate high frequency variability, the 6-hourly gridded data was first processed to yield monthly means. The EOFs were computed using these monthly means. Also to avoid the masking of *inter-ocean* variability patterns, instead of pursuing a global EOF analysis, a separate analysis in the Pacific, Atlantic, and Indian Oceans, including their respective Southern Ocean sectors, was performed. The first two EOF patterns (EOF1 and EOF2) were computed for DJF, and JJA, although only the EOF1s are shown here. The explained variability of all the EOFs mentioned in this study are presented in Table 1.

Figures 4(A-I) and 5(A-I) show the DJF and JJA spatial patterns of the EOF1 of H_s , H_s^s , and H_s^w , for the Pacific, Atlantic, and Indian Oceans. The spatial patterns of the leading modes of H_s , H_s^s , and H_s^w are qualitatively comparable in the Pacific and Atlantic Oceans in both seasons. In these

Table 1 – Empirical Orthogonal Functions – explained variability of EOF1 and EOF2 (in %).

	EOF1						EOF2					
	DJF			JJA			DJF			JJA		
	H_s	H_s^S	H_s^W									
Pacific	70.9	77.8	63.5	58.1	68.0	67.4	-	-	-	-	-	-
Atlantic	52.1	59.3	62.6	70.5	79.3	60.7	-	-	-	-	-	-
Indian	56.3	70.1	74.2	66.0	77.8	61.9	-	-	-	-	-	-
North Pacific	70.9	77.8	63.5	58.1	68.0	67.4	29.0	22.1	36.4	41.8	31.9	32.5
North Atlantic	52.1	59.3	62.6	70.5	79.3	60.7	47.8	40.6	37.3	29.4	20.6	39.2
Southern Ocean	71.0	69.4	76.2	63.7	66.6	62.9	22.1	17.4	31.4	31.8	28.4	38.6

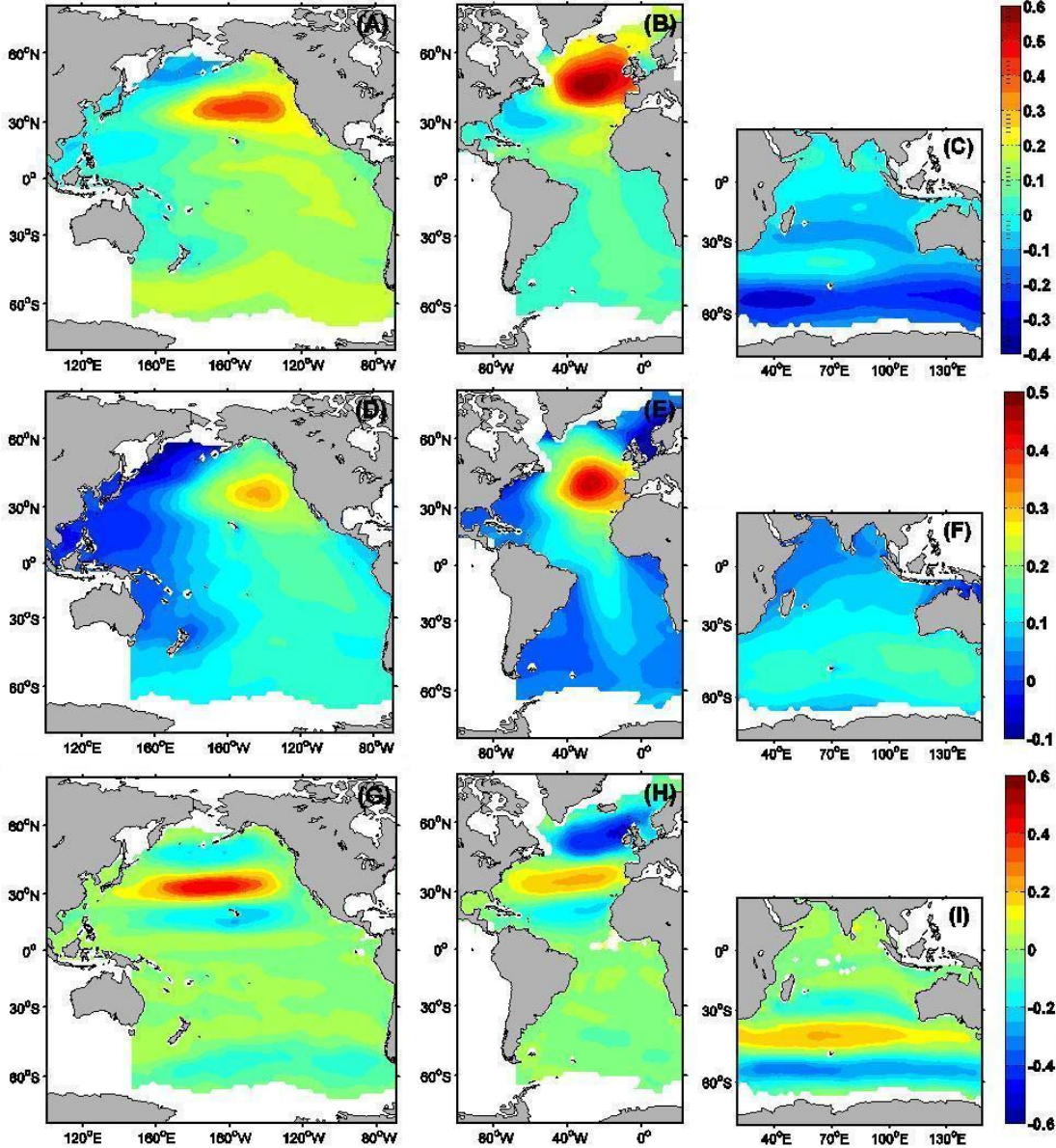


Figure 4- First EOFs of DJF detrended significant wave height (A)-(C), swell significant wave height (D)-(E) and wind sea significant wave height (G)-(I) for the Pacific, Atlantic and Indian oceans. The color scales vary between the sub-figures.

Oceans, in DJF, the EOF1s patterns of H_s (Figures 4A and 4B) are formed by anomalies of the same sign dominating throughout almost the all basins. The maximum explained variances are observed along the central and East subpolar areas. In the South Pacific, in the extratropic belt, the wave-like pattern of the dominating sign is similar to the feature found by Alves (2006) in his numerical experiment of swell propagation patterns. The EOF1s patterns of H_s^s (Figures 4D and 4E) are also formed by dominating anomalies of the same sign. These patterns clearly represent eastward and southward swell propagating from the Northern extratropics storm track regions. In the Pacific Ocean the southward development of the H_s^s field dominating pattern of variability, extends until about 60°S, propagating as far as the West coast of Chile. In the Atlantic Ocean the southward swell propagation pattern reaches the Northwest coast of Brazil, the coasts of Namibia and South Africa, and as far as 60°S. Apparently, although limitative, the geography of the Atlantic Ocean does not prevent swell waves to propagate South. The EOF1s patterns of the H_s^w fields in DJF in both Oceans (Figures 4G and 4H) are characterized by a well defined meridional tripole. The main patterns of variability of H_s , H_s^s and H_s^w in the Indian Ocean are different from the Pacific and Atlantic Oceans. The pattern of the EOF1 of H_s , in DJF (Figure 9C), exhibits a tripole structure centered around 40° S, and is qualitatively more influenced by the variability modes of the H_s^w field than in the remaining Oceans. The spatial pattern of this structure is formed by anomalies of the same sign around 60°S and 30°S, and anomalies of the opposite sign in the subtropics.

The JJA spatial patterns of the EOF1 of H_s , H_s^s and H_s^w in the Pacific, Atlantic, and Indian Oceans are shown in Figure 5(A-I). Some symmetry with the DJF EOF1 patterns can be found. Nevertheless, the rougher JJA wave climate in the Southern Ocean dictates some fundamental differences. The EOF1 of H_s (Figure 5A), in the Pacific Ocean, is formed by anomalies of the same sign in most of the basin, developing from the subpolar latitude in the South Pacific towards the North American Continent. In the Atlantic Ocean the H_s EOF1 pattern is also formed by dominating anomalies of the same sign. A secondary center of action in the North Atlantic, along the extratropical storm area, is present. The EOF1s patterns of H_s^s in these oceans (Figure 5D and 5E) exhibit dominating anomalies of the same sign, extending northward from the South extratropical areas, throughout almost the all basins. The EOF1s patterns of the H_s^w fields (Figure 5G) also exhibits a meridional tripole. The EOF1 of the H_s field in the Indian Ocean (Figure 5C) exhibits a similar pattern to the Pacific and Atlantic oceans. It is dominated by anomalies of the same sign, originated in a meridionally developed center of action, located in the subpolar region. These anomalies extend trough the all basin, decreasing in magnitude towards the North. The EOF1 patterns of the H_s^s field (Figure 9F) is formed by anomalies of the same sign, throughout the all basin, with a strong development towards

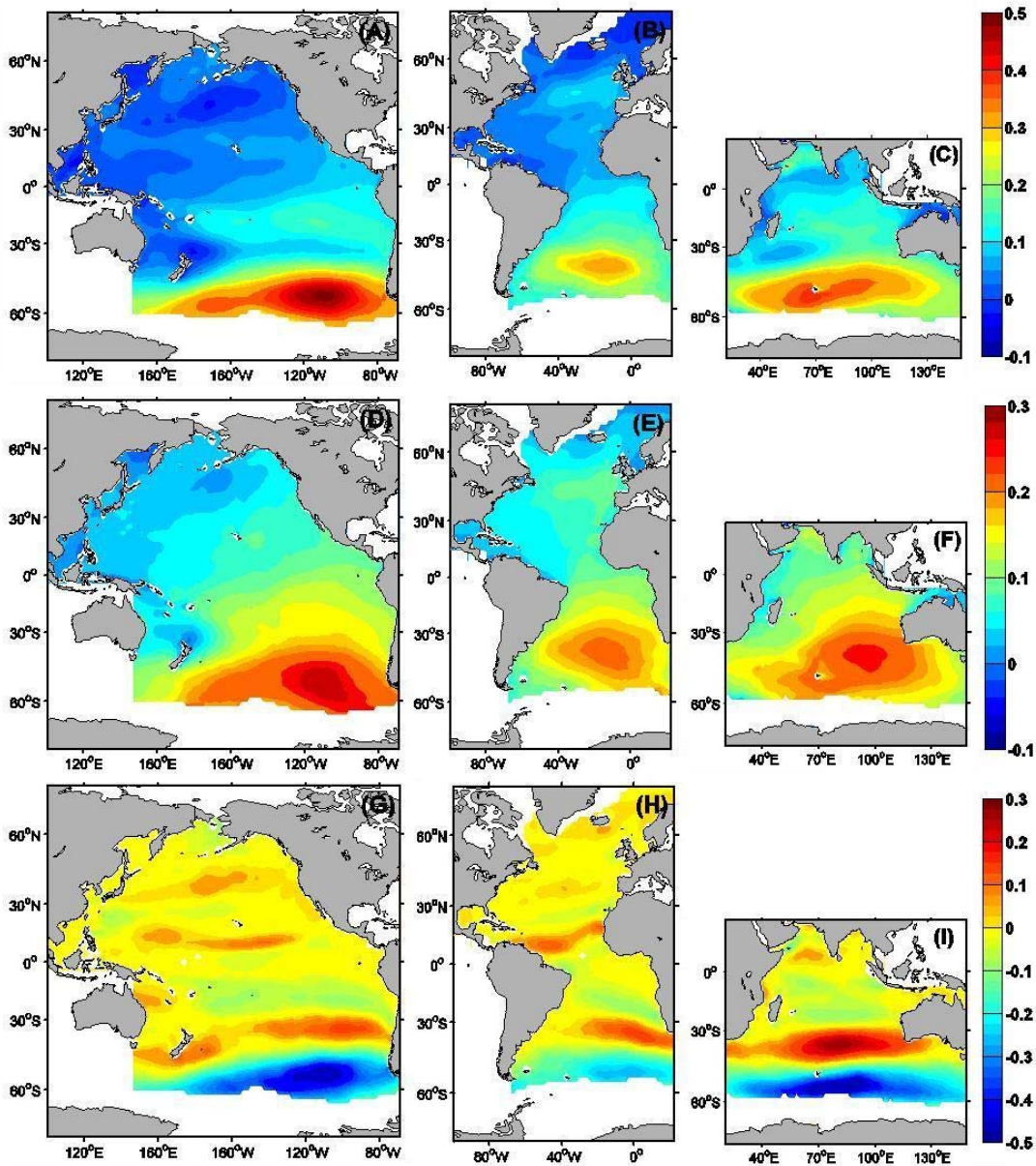


Figure 5 - First EOFs of JJA detrended significant wave height (A)-(C), swell significant wave height (D)-(E) and wind sea significant wave height (G)-(I) for the Pacific, Atlantic and Indian oceans. The color scales vary between the sub-figures.

South Australia. The EOF1 of the H_s^w (Figure 5I) reveals a spatial pattern similar to DJF, with a tripole structure, but with higher variability.

To analyze the association between the wave height variability and the atmospheric circulation patterns, an additional EOF analysis is performed to the detrended seasonal means of the H_s , H_s^s and H_s^w regional fields. The DJF and

JJA EOF1 and EOF2, and principal components (PC1 and PC2) are computed separately for the North Atlantic and North Pacific sub-basins, and for the Southern Ocean belt. The explained variance can be seen in Table 2. The atmospheric circulation patterns are represented by atmospheric indices (the atmospheric drivers): the North Atlantic Oscillation (Hurrell, 1995), the North Pacific Index (Trenberth and Hurrell, 1994), the Southern Oscillation Index (Ropelewski and Jones, 1987), and the Southern Annular Mode Index (Marshall, 2003). The strength of the North Atlantic and Northeastern Pacific westerlies can be deduced from the North Atlantic Oscillation (NAO) index and from the North Pacific Index (NPI), respectively. The intensity of the extratropical circulation in the Pacific Ocean is related to the Southern Oscillation, represented by the Southern Oscillation Index (SOI), through the mechanism of the “atmospheric bridge” (Alexander *et al.*, 2002). The SAMI represents the principal mode of variability in the atmospheric circulation of the Southern Ocean extratropics and high latitudes, and is related to the Southern Ocean belt wind regime (Hurrell and van Loon, 1994).

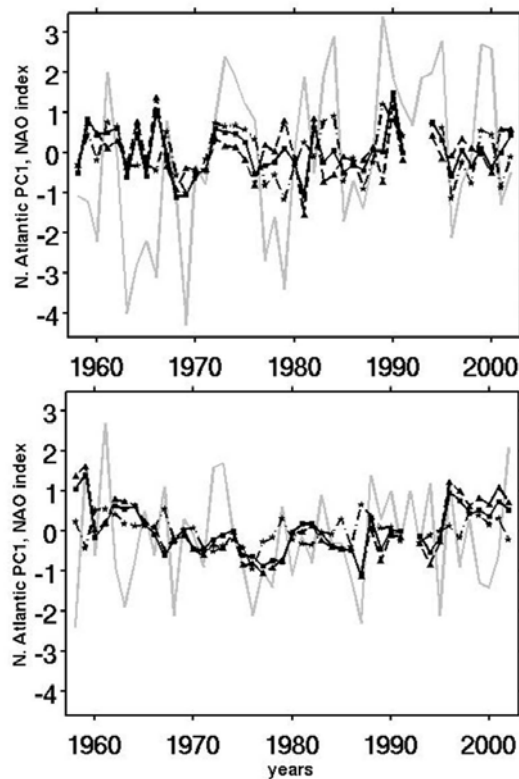


Figure 6 - First normalized PCs of DJF (top) and JJA (bottom) detrended H_s (full line with squares), H_s^S (dashed line with triangles), and H_s^W (dot-dashed line with stars), in the North Atlantic, along with the NAO index (gray line).

Figure 6 displays the North Atlantic DJF and JJA H_s , H_s^s and H_s^w PC1 time series, and the NAO index. The correlation coefficients of the H_s , H_s^s and H_s^w principal components (PC1 and PC2), with each other and with the NAO index, are shown in Table 2. GG06 followed a similar approach. Here we choose to show the full ERA-40 period only, but include both PC1 and PC2, and the respective summer analysis. In the North Atlantic the H_s^w and H_s^s PCs are always poorly correlated, with the exception of the PC2, in JJA ($r=0.63$). The correlation between the first leading modes of H_s^w and H_s is low in both seasons.

Table 2 - Correlation coefficients of the first and second PCs of H_s , H_s^s , and H_s^w , in the North Atlantic, with each other and with the NAO index, for DJF and JJA.

Pairs of parameters	EOF1		EOF2	
	DJF	JJA	DJF	JJA
$H_s^w - H_s^s$	0.13	0.24	0.26	0.63
$H_s^w - H_s$	0.48	0.14	0.56	0.68
$H_s^s - H_s$	0.81	0.98	0.88	0.98
H_s^w -NAO	0.84	0.07	0.26	0.51
H_s^s -NAO	0.30	0.08	0.87	0.59
H_s -NAO	0.26	0.15	0.85	0.56

seasons. Nevertheless, the correlation between their PC2s is higher, especially in JJA ($r=0.68$). The correlation between the H_s and H_s^s PCs is relatively high or very high, independently of the season ($r>0.80$). The low correlation between the H_s^w and H_s^s reflects the swell propagation effect, since locally generated waves are not necessarily correlated with swell waves. An exception might be during dynamic fetch situations when swell waves “travel” with the storm. The higher agreement between H_s and H_s^s is, again, a consequence of the swell dominance of the wave spectra. The high seasonality of the U_{10} climate in the North Atlantic is reflected in the low correlation between H_s and H_s^w in JJA, and very high correlation between H_s and H_s^s , in the same season. The H_s^w PC1 is highly correlated with the NAO index in DJF ($r=0.84$), but not in JJA ($r=0.07$). The agreement between the H_s and H_s^s PC1s and the NAO index is low in both seasons ($r=0.30$, and $r=0.26$, respectively). As seen in Figure 4 the spatial patterns of the EOF1 of H_s^w , in the North Atlantic in DJF, exhibits a NAO-like structure. On the other hand the spatial patterns of the EOF1 of H_s^s in the same

season clearly represent swell propagating away from the storm track region, and are not related to the NAO. Since H_s is dominated by swell, its PC1 is also not related to the NAO. On the other hand the DJF H_s and H_s^s PC2s have a correlation of 0.85 and 0.87, with the NAO index, respectively. These results are in line with Sterl and Caires (2004), but not with the findings of GG06. It appears that the variability modes of the wind sea and swell heights estimates from VOS are more correlated with each other, and therefore swell “follows” the wind sea pattern and its NAO-like structure. An explanation can be in the subjective judgment of the observer, that is intuitively driven to correlate wind sea and swell in his visual estimate of the wave heights. In JJA the correlation between the H_s , H_s^s , and H_s^w leading modes and the NAO index is very low, revealing that the effect of the strength of the North Atlantic summer westerlies in the wave height variability is rather low.

The time series of the H_s , H_s^s , and H_s^w first leading modes in the North Pacific, for DJF and JJA, along with the NPI and SOI, are shown in Figure 7. The H_s , H_s^s , and H_s^w PC1 and PC2 correlation coefficients, between them selves and with the NPI and SOI, are shown in Table 3. The most striking thing in the North

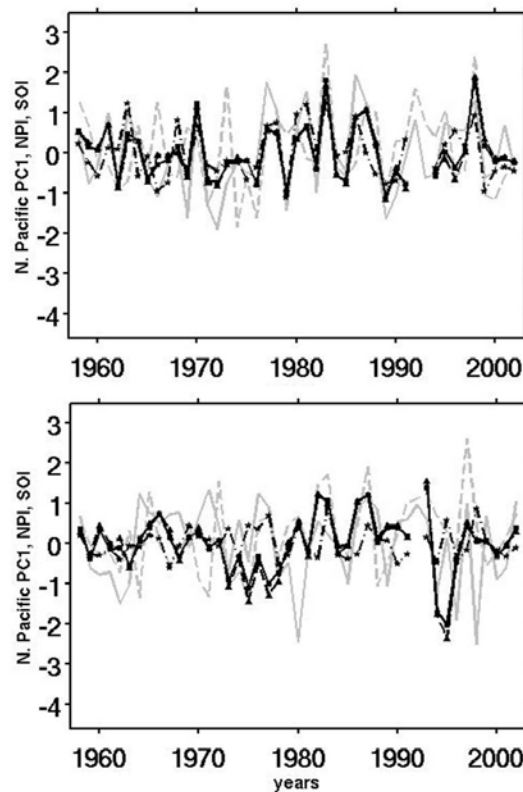


Figure 7 - First normalized PCs of DJF (top) and JJA (bottom) detrended H_s (full line with squares), H_s^s (dashed line with triangles), and H_s^w (dot-dashed line with stars), in the North Pacific, along with the NPI (gray line) and SOI (dashed gray line).

Pacific is the almost perfect correlation (close to 1) between the H_s , and H_s^s PC1s in both seasons. Indeed the variability of the North Pacific wave field is mostly dominated by the swell variability all year round. The correlation between the H_s^s and H_s^w PC1s is higher in the North Pacific ($r=0.54$), than in the North Atlantic in DJF, but close to zero in JJA. The H_s^s and H_s^w PC2s have a low correlation in both seasons. The correlation between the first leading modes of H_s^w and H_s show some agreement in DJF ($r=0.64$), but is close to zero in JJA.

Table 3 - Correlation coefficients of the first and second PCs of H_s , H_s^s , and H_s^w , in the North Pacific, with each other and with the NPI and SOI, for DJF and JJA.

Pairs of parameters	EOF1		EOF2	
	DJF	JJA	DJF	JJA
$H_s^w - H_s^s$	0.54	-0.05	0.35	0.39
$H_s^w - H_s$	0.64	0.03	0.35	0.52
$H_s^s - H_s$	0.99	0.99	0.47	0.94
H_s^w -NPI	0.78	0.06	0.61	0.50
H_s^s -NPI	0.79	0.23	0.02	0.10
H_s -NPI	0.83	0.29	0.37	0.15
H_s^w -SOI	0.28	0.18	0.57	0.37
H_s^s -SOI	0.57	0.38	0.37	0.19
H_s -SOI	0.57	0.41	0.05	0.21

The correlation between the H_s , H_s^s , and H_s^w PC1s and the NPI is high in DJF ($r=0.83$, $r=0.79$, and $r=0.78$, respectively) and low in JJA ($r<0.3$). The correlation between H_s^w and the H_s and H_s^s PC2 and the NPI is very low in both seasons, but the correlations between H_s^w PCs and the NPI is significant ($r>0.5$) in both seasons. The DJF results are very much in line with GG06, although our results show a slightly higher correlation between the H_s , H_s^s , and H_s^w leading modes and the NPI. The correlation between the SOI and the H_s , H_s^s , and H_s^w PCs appears to be low. The exceptions are H_s and H_s^s in DJF, with $r=0.57$, and the H_s^w PC2, with $r=0.57$. The Southern Oscillation does have some impact in the North Pacific wave variability (more in DJF), most probably in swell waves generated along the trade winds path.

The Southern Ocean H_s , H_s^s , and H_s^w PC1s, along with the SAMI, for DJF and JJA, are displayed in Figure 8. The H_s , H_s^s , and H_s^w PC1 and PC2 correlation coefficients, between them selves and with the SAMI, are shown in

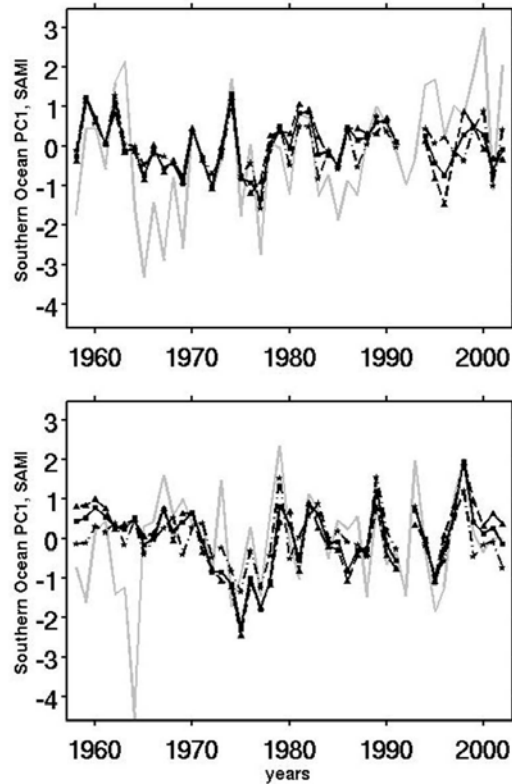


Figure 8 - First normalized PCs of DJF (top) and JJA (bottom) detrended H_s^w (full line with squares), H_s^s (dashed line with triangles), and H_s (dot-dashed line with stars), in the Southern Ocean belt, along with the SAMI (gray line).

Table 4. The agreement between the H_s and H_s^s PCs is high in both seasons, and similar to the NH ($r \geq 0.87$). The correlation between the H_s^w and H_s^s PC1s is not very strong ($r=0.49$ and $r=0.58$, in DJF and JJA, respectively). The correlation between the H_s^w and H_s PC1s is high in both seasons ($r=0.78$ and $r=0.75$, in DJF and JJA, respectively). These correlation results show the regularity and low seasonality of the Southern Ocean wave heights climate, although slightly more wind sea dominated during the SH winter. The correlation pairs of H_s , H_s^s , and H_s^w in the separate Southern Ocean sectors (not shown here) are very similar, although slightly lower in the Indian sector, especially in JJA.

The correlation between the H_s^w PC1s and the SAMI is high in DJF ($r=0.73$), but lower in JJA ($r=0.51$). The correlations between the H_s^s PCs and PC1 and the SAMI is relatively high in DJF ($r=0.60$), but lower in JJA ($r=0.49$). The correlations between the wave height parameters PCs and the SAMI (not shown here) in the Southern Ocean sectors are relatively similar: slightly higher in the Indian Sector, in JJA, and lower in the Atlantic Sector in both seasons.

Table 4 - Correlation coefficients of the first and second PCs of H_s , H_s^s , and H_s^w , in the Southern Ocean belt with each other and with the SAMI, for DJF and JJA.

Pairs of parameters	EOF1		EOF2	
	DJF	JJA	DJF	JJA
$H_s^w - H_s^s$	0.49	0.58	0.04	0.39
$H_s^w - H_s$	0.78	0.75	0.22	0.21
$H_s^s - H_s$	0.92	0.97	0.87	0.94
H_s^w -SAMI	0.73	0.49	0.04	0.14
H_s^s -SAMI	0.37	0.28	0.11	0.27
H_s -SAMI	0.57	0.37	0.03	0.11

To the best of the authors' knowledge, the only SH ocean-scale regional wave climate study focusing on the wave climate interannual variability is the recent study from Hemer *et al.* (2009). They have used a 19 years long remote sensing wave height data set, blended with ERA-40 mean directions. Our results show some qualitative agreement with Hemer *et al.* (2009) results, mainly the correlation between the H_s PC1 and the SAMI, and the low correlation between the South Atlantic H_s modes of variability and the SAMI. But some disagreements are also worth of notice, like the fact that in our study the correlation between the H_s PC1 and the SAMI is high in DJF (actually higher than in JJA), which is not in line with their findings.

5. Summary and conclusions

By taking advantage of the flexibility of the ERA-40 wave reanalysis, a detailed climatology of the global DJF and JJA wind sea and swell significant wave heights.

The interannual variability of the wind sea and swell significant wave heights was investigated by means of an EOF analysis. The propagating patterns of swell in the Pacific, Atlantic, and Indian Ocean have been studied using a simple correlation analysis. The North-South swell propagation in the Pacific Ocean had been known from previous studies. In the present study evidence was found that the swell propagation pattern in the Atlantic Ocean, despite its narrow geometry, might be stronger than previously thought, especially in DJF from the North Atlantic to the South Atlantic.

To analyze the potential mechanisms behind the interannual variability of the wind sea and swell significant wave heights, the relation between the large scale forcing, represented by several atmospheric drivers has been studied. The influence of the large scale atmospheric patterns has been found to be more influential in the large scale variability of the wind sea and swell significant

heights in the NH during DJF. On the other hand, the strength of the Southern Ocean wind speed, represented by the SAMI, is the most important driving force behind the wave climate in the SH, independently of the season.

Future analysis of the variability of wind sea and swell should go in the direction of the tendencies of the T_m^s and wave power (or wave energy flux), since changes in the energy potential of very long swells generated in the winter hemisphere can have pose a considerable danger to coastal and offshore structures.

Acknowledgments

Alvaro Semedo and Kay Sušelj are funded by the European Commission through a research fellowship under the ModObs project, contract MRTN-CT-2005-019369. We greatly appreciated the support and valuable discussions and critics from Andreas Sterl of KNMI (De Bilt, Netherlands) and Sofia Caires of Deltares - Delft Hydraulics (Delft, Netherlands), and the help of Jean Bidlot from ECMWF (Reading, United Kingdom) with the many details of the ERA-40 wave data.

References

- Alexander, M. A., I. Blade, M. Newman, J. Lanzante, N.-C. Lau, and J. D. Scott (2002), The atmospheric bridge: The influence of the ENSO teleconnections on air-sea interaction over the global oceans, *J. Climate*, **15**, 2205–2231.
- Alves, J.H.G.M, 2006: Numerical modeling of ocean swell contributions to the global wind-wave Climate. *Ocean Modelling*. Vol. 11 (1-2), 98-122.
- Ardhuin, F. and A. D. Jenkins, 2006: On the interaction of surface waves and upper ocean turbulence. *J. Phys. Oceanogr.*, **36**, 551–557.
- , B. Chapron, F. Collard, 2009: Strong dissipation of steep swells observed across oceans. *G. Research Letters*- in press.
- Caires, S. A. Sterl, and C. P. Gommenginger 2005, Global ocean mean wave period data: Validation and description, *J. Geophys. Res.*, **110**, C02003, doi:10.1029/2004JC002631.
- Chen, G., R. Ezraty, C. Fang, and L. Fang, 2002: A new look at the zonal pattern of the marine wind system from TOPEX measurements. *Remote Sens. Environ.*, **79**, 15–22.
- Donelan, M.A., Drennan, W.M., Katsaros, K.B., 1997. The air–sea momentum flux in conditions of wind sea and swell. *J. Phys. Oceanogr.* **27** (10), 2087–2099.
- Gerling, T.W., 1992: Partitioning sequences and arrays of directional wave spectra into component wave systems. *J. Atmos. Ocean. Technol.*, **9**, 444–458.

- Grachev, A.A., Fairall, C.W., 2001: Upward momentum transfer in the marine boundary layer. *J. Phys. Oceanogr.*, **31**,1698–1711.
- Gulev, S. K., V. Grigorieva, A. Sterl, and D. Woolf. 2003: Assessment of the reliability of wave observations from voluntary observing ships: Insights from the validation of a global wind wave climatology based on voluntary observing ship data, *J. Geophys. Res.*, **108(C7)**, 3236, doi:10.1029/2002JC001437.
- , and V. Grigorieva, 2006: Last century changes in ocean wind wave height from global visual wave data, *Geophys. Res. Lett.*, **31**, I24302, doi:10.1029/2004GL021040.
- Hemer, M.A., J.A Church, J.R. Hunter, 2009: Variability and trends in the directional wave climate of the Southern Hemisphere. *Int. J. Climatol.*, in press.
- Hurrell, J.W., van Loon H., 1994: A modulation of the atmospheric cycle in the Southern Hemisphere. *Tellus*, **64A**, 325-338.
- ,1995: Decadal trends in the North Atlantic Oscillation: regional temperatures and precipitation. *Science*, **269**, 676-679.
- Kantha, L., 2006: A note on the decay rate of swell. *Ocean Modelling*, **11**, 167–173.
- Komen, G. J., L. Cavaleri, M. Doneland, K. Hasselmann, S. Hasselmann, and P. A. E. M. Janssen, (Eds.), 1994: Dynamics and Modelling of Ocean Waves. Cambridge University Press.
- Marshall, G.J., 2003: Trends in the southern annular mode from observations and reanalyses. *J. Climate*, **16**, 4134–4143.
- Munk, W.H., 1945: Tracking storms by forerunners of swell, *J. Meteorol.*, **4**(2), pp. 45–57.
- , 1951: Origin and generation of waves. Proc. First Coastal Engineering Conference, Long Beach, Calif., 1–4.
- Ropelewski, C. F., and P. D. Jones (1987), An extension of the Tahiti-Darwin Southern Oscillation Index, *Mon. Weather Rev.*, **115**, 2161–2165.
- Semedo, A., Sætra, Ø., Rutgersson, A., Kahma, K., Pettersson, H.: Wave induced wind in the marine boundary layer. *J. Atmos. Sci*, **66**, 2256-2271.
- Smedman, A.-S., U. Högström, H. Bergström, A. Rutgersson, K. K. Kahma, and H. Petterseon,1999: A case study of air-sea interaction during swell conditions. *J. Geophys. Res.*, **104**, 25833–25851.
- , A., U. Högström, E. Sahleé, W. M. Drennan, K. K. Kahma, H. Pettersson, and F. Zhang, 2009: Observational study of marine atmospheric boundary layer characteristics during swell. *J. Atmos. Sci.*, **66**, 2747–2763.

- Trenberth, K. E., and J. W. Hurrell (1994), Decadal atmosphere-ocean variations in the Pacific, *Clim. Dyn.*, **9**, 303–319.
- Uppala, S. M., and Coauthors, 2005: The ERA-40 re-analysis. *Quart. J. Roy. Meteor. Soc.*, **131**, 2961–3012.
- von Storch, H. and F. Zwiers, 1999: *Statistical Analysis in Climate Research*. Cambridge Univ. Press, New York, 494 pp.
- Young I. R., 1999: Seasonal variability of the global ocean wind and wave climate. *Int. J. Climatol.*, **19**, 931–950.
- WAMDI Group, 1988: The WAM Model - A Third Generation Ocean Wave Prediction Model. *J. Phys. Oceanogr.* **18**, 1775-1810.